applied sciences

MDPI

Article

# Evolutionary Algorithm-Based Friction Feedforward Compensation for a Pneumatic Rotary Actuator Servo System

**Ke Li *, Yeming Zhang *, Shaoliang Wei * and Hongwei Yue**

School of Mechanical and Power Engineering, Henan Polytechnic University, Jiaozuo 454000, China; 15239178258@163.com

* Correspondence: leeketech@163.com (K.L.); tazhangyeming@163.com (Y.Z.); wsl_ify@163.com (S.W.)

Received: 22 August 2018; Accepted: 7 September 2018; Published: 12 September 2018

check for updates

**Abstract:** The friction interference in the pneumatic rotary actuator is the primary factor affecting the position accuracy of a pneumatic rotary actuator servo system. The paper proposes an evolutionary algorithm-based friction-forward compensation control architecture for improving position accuracy. Firstly, the basic equations of the valve-controlled actuator are derived and linearized in the middle position, and the transfer function of the system is further obtained. Then, the evolutionary algorithm-based friction feedforward compensation control architecture is structured, including that the evolutionary algorithm is used to optimize the controller coefficients and identify the friction parameters. Finally, the contrast experiments of four control strategies (the traditional PD control, the PD control with friction feedforward compensation without evolutionary algorithm tuning, the PD control with friction feedforward compensation based on the differential evolution algorithm, and the PD control with friction feedforward compensation based on the genetic algorithm) are carried out on the experimental platform. The experimental results reveal that the evolutionary algorithm-based friction feedforward compensation greatly improves the position tracking accuracy and positioning accuracy, and that the differential evolution-based case achieves better accuracy. Also, the system with the friction feedforward compensation still maintains high accuracy and strong stability in the case of load.

**Keywords:** pneumatic rotary actuator; position accuracy; friction feedforward compensation; differential evolution algorithm; genetic algorithm

## 1. Introduction

Pneumatic technology has the advantages of fire prevention, energy saving, high efficiency and no pollution [1–4]. It has become an important means to realize the automation of production process with the complement of hydraulic, mechanical, electrical and electronic technology [5–8]. Also, pneumatic servo systems have been widely used in the proportional control and program control systems in some multipipe production processes of automobile production lines, as well as the metallurgy and chemical industries [9]. Among them, the pneumatic rotary actuator can rotate in a plane, therefore the pneumatic rotary actuator servo system is indispensable in the rotating occasions such as the pneumatic manipulator, the rotation of the platform and the rotation of the valve [10].

With the increasing demand for the servo performance of the pneumatic rotary actuator servo system in precision industry, the traditional control methods cannot meet the actual requirements gradually [11,12]. The factors affecting the position accuracy of the pneumatic rotary actuator servo system are mainly the dead zone characteristic of the proportional valve and the friction of the actuator [13]. However, at present, the terminal pressures of such pneumatic systems in industry are usually below 1 MPa, hence the studied system is a low speed system with small flow rate. By testing the proportional valve commonly used in this system, we have come to the conclusion that the dead zone characteristic of the proportional valve is not obvious, that is, the proportional valve can quickly change the flow rate of the two valve ports when the spool is slightly moved in the middle position. However, the small-range actuator has a large friction-to-drive ratio, which especially affects the low speed servo performance of the actuator, therefore, friction is the most important factor affecting the position accuracy.

Over the past 400 years, numerous experimental studies have revealed abundant behavior characteristics of friction, such as Coulomb friction, viscous friction, static friction, Stribeck effect [14], pre-sliding. Because of the nonlinear characteristics of friction [15], how to minimize the impact of friction becomes a challenging task. Therefore, the topic of the friction prediction, identification and compensation is one of the hotspots of current research.

The compensation control for friction can be divided into the non-model friction compensation and the model-based friction compensation. The nonmodel friction compensation mainly relies on the control algorithm to identify the deviation caused by friction and compensates for the system. Gao [16] designed a new friction compensator based on the adaptive Fuzzy-PD control algorithm, it can adaptively adjust the controller parameters according to the change of output error and error change rate, so as to accurately control the pneumatic servo system. In the application of the model-based friction compensation, Meng [17] constructed an adaptive robust controller with LuGre model-based friction compensation, which can effectively solve the problems of unmodeled dynamics and friction disturbances in the pneumatic system and showed better results than other studies. The model-based friction compensation has the ability of friction prediction, hence it has a more significant friction compensation effect and has a more extensive application.

At present, many scholars have proposed various friction models, which can be divided into two categories: the dynamic friction model and the static friction model. The dynamic friction model describes friction as a function of relative velocity and displacement [15], such as LuGre friction model. The paper [18] presents the application of the LuGre friction model to the friction compensation scheme of a pneumatic servo system, where the friction parameters are determined by using adaptive estimation instead of extensive identification procedures. In addition, Raul [19] built a cascade controller with the LuGre model-based friction compensation, which can effectively control the tracking error of the pneumatic system under the premise that the system parameters were known. The static friction model, another category of friction models, describes friction as a function of relative velocity [20], and the Stribeck model is the most commonly used one. Over the years, the Stribeck friction model has made good progress in the servo system. In paper [21], the friction of the hydraulic actuator are well described by the Stribeck friction model whose friction parameters are identified by the proposed iterative algorithm, and the proposed scheme applies to industrial systems due to its low computational cost. Furthermore, Castro [22] proposed a controller including the friction compensation based on the Stribeck friction model, and the controller achieved great stability and robustness in the hybrid brake-by-wire system. The displacement of a pneumatic actuator is difficult to control, which results in the difficulty of identifying the dynamic parameters in the dynamic friction model, therefore the use of the static friction model is more conducive to the identification and compensation in the pneumatic rotary actuator servo system.

The proportional–integral–derivative (PID) control is an effective method which can dynamically reduce the output deviation of a servo system, where proportional–derivative (PD) control can reduce the system delay and is suitable for high-speed control of the proportional valve [23]. Besides, evolutionary algorithms, such as differential evolution (DE) algorithm and genetic algorithm (GA), can optimize the controller parameters [24,25] and identify the friction parameters [26,27], and have been used in friction feedforward compensation. At present, the evolutionary algorithm-based friction feedforward compensation has been applied to the direct-current servo system, and shows great performance [26,27]. Therefore, the application of evolutionary algorithm-based friction feedforward compensation has broad prospects in the pneumatic rotary actuator servo field.

In order to improve the position accuracy of the pneumatic rotary actuator servo system, the modeling of the system and the design of the evolutionary algorithm-based friction feedforward compensation control architecture are carried out and verified by the experiments in this paper. Among them, the linearized model of the system with Stribeck friction model and the construction of the friction feedforward compensation control architecture are described in detail. Evolutionary algorithms (DE and GA) are applied to the parameter optimization of the control architecture to further improve the system control accuracy. The control performances of four control strategies (the traditional PD control, the PD control with friction feedforward compensation without evolutionary algorithm tuning, the PD control with friction feedforward compensation based on the DE algorithm and the PD control with friction feedforward compensation based on the GA) are contrasted by the experiments which include the position tracking experiment, the positioning experiment and the stability experiment with load. The experimental results reveal that the evolutionary algorithm-based friction feedforward compensation greatly improves the position tracking accuracy and positioning accuracy, and that the DE-based case achieves better accuracy. Also, the system with the friction feedforward compensation still maintains high accuracy and strong stability in the case of load.

## 2. System Configuration

Figure 1 illustrates the system configuration of the pneumatic rotary actuator servo system. The compressor and the air service unit produce compressed air to provide sufficient kinetic energy for the pneumatic system. The air service unit is added to the system to filter compressed air and regulate pressure. The control valve used in the system is a 5/3-way proportional directional control valve, which can control the rotational motion of the actuator by changing the flow and direction of the valve port gas. In order to improve the control accuracy, the feedback link is necessary in the system, where the data acquisition card receives the rotation angle signal (TTL levels) collected by the rotary encoder and outputs the voltage signal of 0–10 V to the proportional directional control valve to accurately change the flow of the valve port gas again. In addition, the data acquisition card is installed in the industrial personal computer (IPC), and accepts the control instructions of the host computer based on LabVIEW. The specific models of the main components are presented in Table 1.

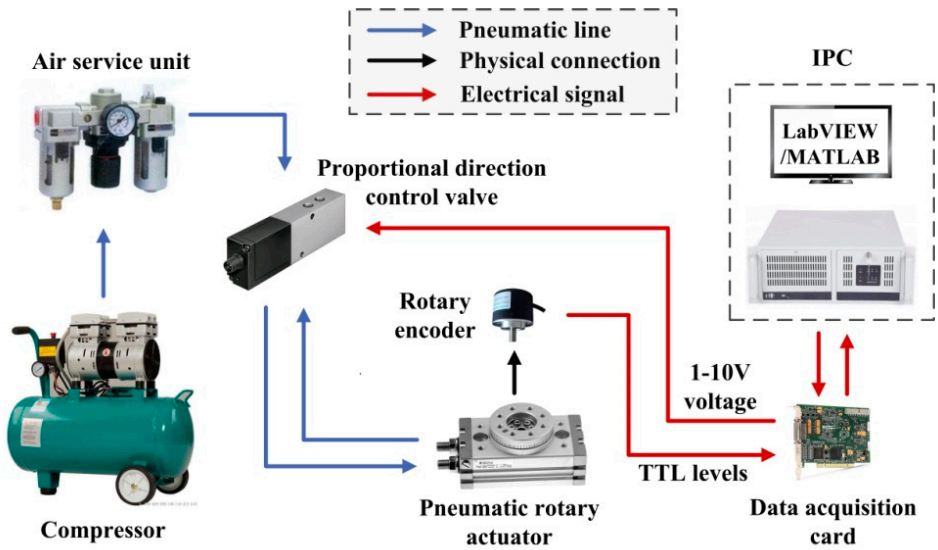


**Figure 1.** System configuration of the pneumatic rotary actuator servo system.

**Table 1.** The specific models of the main components.

| Component | Model | Parameters |
|---|---|---|
| Compressor | PANDA 750-30L | Maximum supply pressure: 0.8 MPa |
| Air service unit | AC3000-03 | Maximum working pressure: 1.0 MPa |
| Proportional directional control valve | FESTO MPYE-5-M5-010-B | 5/3-way valve, 0~10 V driving voltage |
| Pneumatic rotary actuator | SMC MSQA30A | Bore: 30 mm; stroke: 190° |
| Rotary encoder | E58S10 | Resolution: 36000 P/R |
| Data acquisition card | NI PCI-6229 | 32-bit counter; −10~10 V voltage output |
| IPC | IPC-610H | Standard configuration |

## 3. System Modeling

Figure 2 describes the gas flow mechanism in the valve-controlled actuator system. The mass flow rates of the gas flowing through the two valve ports are $\dot{M}_a$ and $\dot{M}_b$, the gas pressures in the two chambers are $p_a$ and $p_b$, the gas volumes are $V_a$ and $V_b$, and the gas temperatures are $T_a$ and $T_b$. In addition, $p_s$ represents the supply pressure, $x_v$ and $y$ stand for the valve spool displacement and the actuator piston displacement respectively, and $\theta$ is the rotation angle of the actuator.

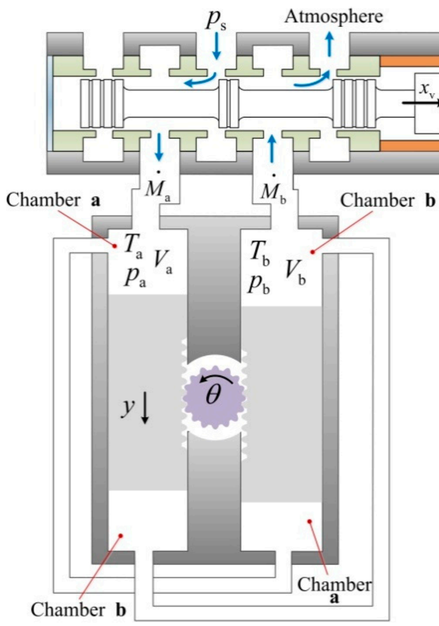


**Figure 2.** Gas flow mechanism in the valve-controlled actuator system.

As shown in Figure 2, the two valve ports of the proportional valve are connected with the two chambers of the actuator respectively. When the valve spool moves to the right, chamber **a** is charged, and chamber **b** is discharged. The two-chamber pressure difference drives the piston to move and converts the linear motion into the rotational motion of the intermediate gear. Before the system modeling, we need to make the following assumptions [28–30]:

(1) The working medium is ideal gas, which follows the ideal gas law.
(2) Supply pressure $p_s$ and supply temperature $T_s$ are constant, and the parameter of each point in the chamber is equal at each instant.
(3) There is no leakage between the valve-controlled actuator system and the outside and between the two chambers.
(4) The flow state of the gas flowing through the orifice is an isentropic adiabatic process.
(5) The change of each parameter in the dynamic process is only a small amount (small disturbance hypothesis).

The derivation of the system model begins with the basic equations of the valve-controlled actuator, including the orifice equation of the mass flow rate, the continuity equation of the mass flow rate, and the dynamic equation of the pneumatic rotary actuator [31,32].

### 3.1. Orifice Equation of the Mass Flow Rate

The flow process of the gas passing through the valve port is very complicated. According to the assumptions, the gas flow via the valve port is approximated as one-dimensional isentropic flow of the ideal gas flowing through a orifice [33]. The gas has two states of sonic flow and subsonic flow when passing through the orifice. The mass flow rate of the gas flowing through the proportional valve can be summarized as follows [34].

$$\dot{M}_{\rm a} = \begin{cases} \frac{CWx_{\rm v}p_{\rm s}}{\sqrt{RT_{\rm s}}}\sqrt{\frac{2\kappa}{\kappa-1}\left[\left(\frac{p_{\rm a}}{p_{\rm s}}\right)^{\frac{2}{k}} - \left(\frac{p_{\rm a}}{p_{\rm s}}\right)^{\frac{\kappa+1}{\kappa}}\right]} & \frac{p_{\rm a}}{p_{\rm s}} \geq c_0 \\ \frac{CWx_{\rm v}p_{\rm s}}{\sqrt{RT_{\rm s}}}\sqrt{\frac{2\kappa}{\kappa+1}\left(\frac{2}{\kappa+1}\right)^{\frac{2}{\kappa-1}}} & \frac{p_{\rm a}}{p_{\rm s}} < c_0 \end{cases} \tag{1}$$

$$\dot{M}_{\rm b} = \begin{cases} \frac{CWx_{\rm v}p_{\rm b}}{\sqrt{RT_{\rm b}}}\sqrt{\frac{2\kappa}{\kappa-1}\left[\left(\frac{p_{\rm e}}{p_{\rm b}}\right)^{\frac{2}{\kappa}} - \left(\frac{p_{\rm e}}{p_{\rm b}}\right)^{\frac{\kappa+1}{\kappa}}\right]} & \frac{p_{\rm e}}{p_{\rm b}} \geq c_0 \\ \frac{CWx_{\rm v}p_{\rm b}}{\sqrt{RT_{\rm b}}}\sqrt{\frac{2\kappa}{\kappa+1}\left(\frac{2}{\kappa+1}\right)^{\frac{2}{\kappa-1}}} & \frac{p_{\rm e}}{p_{\rm b}} < c_0 \end{cases} \tag{2}$$

where $C$ represents the discharge coefficient, $W$ stands for the area gradient of the spool valve, $R$ is the gas constant, $\kappa$ is the ratio of the specific heat at constant pressure to the specific heat at constant volume, $p_{\rm e}$ is the atmospheric pressure, and $c_0$ denotes the critical pressure ratio. Then, linearizing Equations (1) and (2) yields

$$\begin{cases} \Delta\dot{M}_{\rm a} = c_1\Delta x_{\rm v} - c_2\Delta p_a \\ \Delta\dot{M}_{\rm b} = -c_1\Delta x_{\rm v} - c_2\Delta p_b \end{cases} \tag{3}$$

where $c_1$ and $c_2$ are both known as zero coefficient. Specifically, $c_1$ is the flow gain, while $c_2$ is the flow-pressure coefficient. Because the spool valve has the same form of the valve port at the left and right ends, the zero coefficients under the initial condition are

$$\begin{cases} c_1 = \left.\frac{\partial\dot{M}_{\rm a}}{\partial x_{\rm v}}\right|_{\substack{p_{\rm a} = p_0 \\ x_{\rm v} = 0}} \approx -\left.\frac{\partial\dot{M}_{\rm b}}{\partial x_{\rm v}}\right|_{\substack{p_{\rm b} = p_0 \\ x_{\rm v} = 0}} \\ c_2 = -\left.\frac{\partial\dot{M}_{\rm a}}{\partial p_{\rm a}}\right|_{\substack{x_{\rm v} = 0 \\ p_{\rm a} = p_0}} \approx -\left.\frac{\partial\dot{M}_{\rm b}}{\partial p_{\rm b}}\right|_{\substack{x_{\rm v} = 0 \\ p_{\rm b} = p_0}} \end{cases} \tag{4}$$

### 3.2. Continuity Equation of the Mass Flow Rate

According to [23], the continuity equation for the mass flow rates of the gas flowing into the two chambers can be expressed as

$$\begin{cases} \dot{M}_{\rm a} = \frac{1}{\kappa RT_{\rm a}}\left(V_{\rm a}\dot{p}_{\rm a} + \kappa p_{\rm a}\dot{V}_{\rm a}\right) \\ \dot{M}_{\rm b} = \frac{1}{\kappa RT_{\rm b}}\left(V_{\rm b}\dot{p}_{\rm b} + \kappa p_{\rm b}\dot{V}_{\rm b}\right) \end{cases}, \tag{5}$$

Under the small disturbance hypothesis, if the initial values are taken in the middle equilibrium position, the following equations can be obtained.

$$\begin{cases} \dot{M}_{\mathrm{a}} = 0 + \Delta\dot{M}_{\mathrm{a}},\ \dot{M}_{\mathrm{b}} = 0 + \Delta\dot{M}_{\mathrm{b}} \\ p_{\mathrm{a}} = p_0 + \Delta p_{\mathrm{a}},\ p_{\mathrm{b}} = p_0 + \Delta p_{\mathrm{b}} \\ V_{\mathrm{a}} = V_0 + \Delta V_{\mathrm{a}},\ V_{\mathrm{b}} = V_0 + \Delta V_{\mathrm{b}} \\ T_{\mathrm{a}} = T_0 + \Delta T_{\mathrm{a}},\ V_{\mathrm{b}} = T_0 + \Delta T_{\mathrm{b}} \end{cases} \tag{6}$$

and

$$\Delta\dot{V}_{\mathrm{a}} = -\Delta\dot{V}_{\mathrm{b}} = A_{\mathrm{p}}\Delta\dot{y} = \frac{1}{2}A_{\mathrm{p}}d_{\mathrm{f}}\Delta\dot{\theta}, \tag{7}$$

where $p_0$, $V_0$ and $T_0$ represent the initial values of the variables, and $T_0$ is equal to the supply temperature $T_{\mathrm{s}}$, and the symbol $\Delta$ stands for the increment caused by the actuator piston deviating from the middle position. The increments $\Delta p_{\mathrm{a}}$, $\Delta p_{\mathrm{b}}$, $\Delta V_{\mathrm{a}}$, $\Delta V_{\mathrm{b}}$, $\Delta T_{\mathrm{a}}$ and $\Delta T_{\mathrm{b}}$ are much smaller than $p_{\mathrm{a}}$, $p_{\mathrm{b}}$, $V_{\mathrm{a}}$, $V_{\mathrm{b}}$, $T_{\mathrm{a}}$ and $T_{\mathrm{b}}$, hence these increments can be ignored in the calculation. Therefore, the incremental form of the mass flow rates can be expressed as

$$\begin{cases} \Delta\dot{M}_{\mathrm{a}} = \frac{1}{\kappa RT_{\mathrm{s}}}\left(V_0\Delta\dot{p}_{\mathrm{a}} + \frac{1}{2}\kappa A_{\mathrm{p}}d_{\mathrm{f}}p_0\Delta\dot{\theta}\right) \\ \Delta\dot{M}_{\mathrm{b}} = \frac{1}{\kappa RT_{\mathrm{s}}}\left(V_0\Delta\dot{p}_{\mathrm{b}} - \frac{1}{2}\kappa A_{\mathrm{p}}d_{\mathrm{f}}p_0\Delta\dot{\theta}\right) \end{cases}. \tag{8}$$

### *3.3. Dynamic Equation of the Actuator*

According to Newton's laws of motion, the dynamic equation of the pneumatic rotary actuator can be expressed by Equation (9).

$$A_{\mathrm{p}}d_{\mathrm{f}}(p_{\mathrm{a}} - p_{\mathrm{b}}) = \left(\frac{1}{2}m_{\mathrm{p}}d_{\mathrm{f}}^2 + J\right)\ddot{\theta} + \frac{1}{2}d_{\mathrm{f}}F_{\mathrm{f}}, \tag{9}$$

where $A_{\mathrm{p}}$ represents the area of thrust surface of the actuator piston, $d_{\mathrm{f}}$ stands for the pitch diameter of the actuator gear, $m_{\mathrm{p}}$ denotes the mass of a single piston, $J$ is the moment of inertia of the gear and the rotary table, $\ddot{\theta}$ is the angular acceleration, and $F_{\mathrm{f}}$ is the friction force on the piston.

Stribeck friction model describes the relationship between friction and speed, which can well characterize the macroscopic characteristics of the friction force in low velocity zone [20]. Stribeck friction model can be described as:

$$F_{\mathrm{f}} = \begin{cases} F_{\mathrm{p}} & \dot{\theta} = 0 \text{ and } \left|F_{\mathrm{p}}\right| < F_f \\ F_{\mathrm{s}}\mathrm{sign}(F_{\mathrm{p}}) & \dot{\theta} = 0 \text{ and } \left|F_{\mathrm{p}}\right| \geq F_f \\ F_{\mathrm{c}}\mathrm{sign}(\dot{\theta}) + (F_{\mathrm{s}} - F_{\mathrm{c}})e^{-(\dot{\theta}/\dot{\theta}_{\mathrm{s}})^2}\mathrm{sign}(\dot{\theta}) + \sigma\dot{\theta} & \left|\dot{\theta}\right| > 0 \end{cases} \tag{10}$$

and

$$F_{\mathrm{p}} = 2A(p_{\mathrm{a}} - p_{\mathrm{b}}), \tag{11}$$

where $F_{\mathrm{p}}$ describes the driving force for the piston, $F_{\mathrm{s}}$ represents the maximum static friction force, $F_{\mathrm{c}}$ denotes the Coulomb friction force, $\dot{\theta}$ is the angular velocity, $\dot{\theta}_{\mathrm{s}}$ is Stribeck velocity, and $\sigma$ is the viscous friction coefficient.

The friction parameters are unknown and can be obtained by the following method [20].

When the pneumatic rotary actuator is static or rotates at constant velocity, there is $\ddot{\theta} = 0$. Therefore, under such conditions, the friction force equation can be obtained from Equation (9) and can be easily measured.

$$F_{\mathrm{f}} = 2A(p_{\mathrm{a}} - p_{\mathrm{b}}). \tag{12}$$

By changing the driving voltage of the proportional valve, we obtain the friction force values at different velocities. As shown in Figure 3, the experimental data obtained can be fitted as the force-velocity curve of the friction model with MATLAB. In order to solve the unknown parameters of Stribeck model, we make two tangents ($f_1$, $f_2$) of the friction curve, as shown in Figure 4. Then we can obtain the friction parameters according to the geometric relationship shown in Figure 4. The maximum value of the friction curve is $F_s$, the slope of the line $f_1$ is the value of $\sigma$, the crossover point of the line $f_1$ and the ordinate axes is $F_c$. A line $f_3$ that is parallel to the abscissa axis is made through $F_c$, and then the abscissa of the crossover point of this line and $f_2$ is $\dot{\theta}_s$. The friction parameters are presented in Table 2.

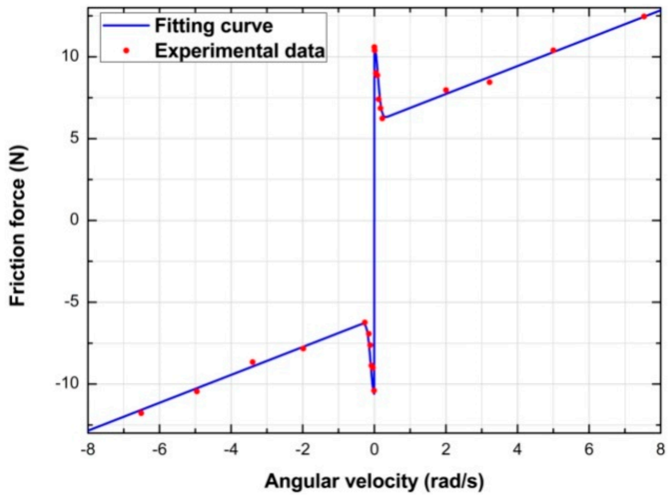


**Figure 3.** Force–velocity curve of the friction model.

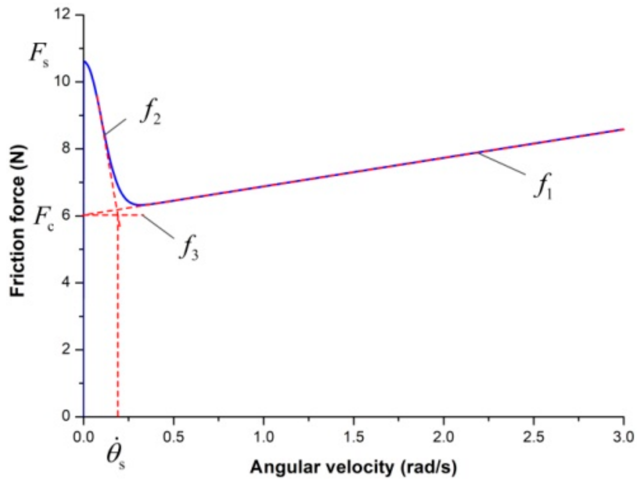


**Figure 4.** Geometric relationship of the friction parameters.

**Table 2.** Values of the friction parameters.

| Friction Parameter | Value |
|---|---|
| $F_s$ | 10.60 (N) |
| $F_c$ | 6.03 (N) |
| $\dot{\theta}_s$ | 0.19 (rad/s) |
| $\sigma$ | 0.87 (N·s·rad$^{-1}$) |

### 3.4. Block Diagram and Transfer Function of the Valve-Controlled Actuator System

Equations (3), (8) and (9) can be transformed into the following form by Laplace transform, respectively.

$$\begin{cases} \dot{M}_a(s) - \dot{M}_b(s) = 2c_1 x_v(s) - c_2[p_a(s) - p_b(s)] \\ \dot{M}_a(s) - \dot{M}_b(s) = \frac{1}{\kappa R T_s}\{V_0 s[p_a(s) - p_b(s)] + \kappa A_p d_f p_0 s\theta(s)\} \\ A_p d_f[p_a(s) - p_b(s)] = \left(\frac{1}{2}m_p d_f^2 + J\right)s^2\theta(s) + \frac{1}{2}d_f F_f(s) \end{cases} \tag{13}$$

From the above equations, we can get the block diagram of the valve-controlled actuator systems shown in Figure 5, where $\dot{M}_1(s) = \dot{M}_a(s) - \dot{M}_b(s)$ denotes the mass flow rate difference and $p_1(s) = p_a(s) - p_b(s)$ stands for the pressure difference. This block diagram also clearly describes the effects of $c_1$, $c_2$ and $F_f$ on the system. In order to facilitate analysis and calculation, we make the following simplification of the system model.

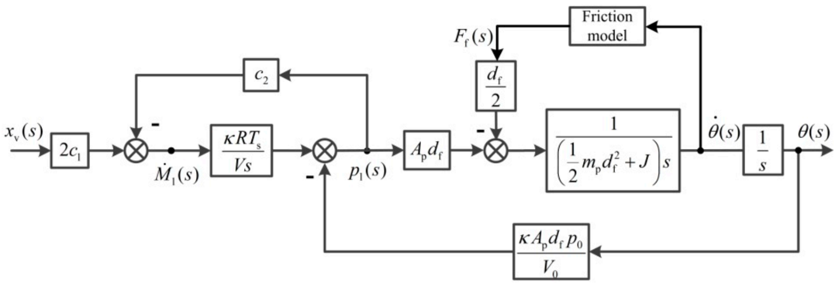


**Figure 5.** Block diagram of the valve-controlled actuator systems.

When $F_f = 0$, we can obtain the transfer function of the displacement $x_v$ to the rotation angle $\theta$, and it can be written as the following standard form.

$$\frac{\theta_x(s)}{x_v(s)} = \frac{K_T\omega_n^2}{s(s^2 + 2\zeta\omega_n s + \omega_n^2)}, \tag{14}$$

where its gain $K_T$, natural frequency $\omega_n$, and damping ratio $\zeta$ are expressed as follows, respectively.

$$\begin{cases} K_T = \frac{2c_1 RT_s}{A_p d_f p_0} \\ \omega_n = \sqrt{\frac{2\kappa A_p{}^2 d_f^2 p_0}{(m_p d_f^2 + 2J)V_0}} \\ \zeta = \frac{1}{2}c_2\kappa RT_s\sqrt{\frac{m_p d_f^2 + 2J}{2\kappa A_p^2 d_f^2 p_0 V_0}} \end{cases}. \tag{15}$$

In addition, we let $x_v(s) = 0$, then we obtain the transfer function of the friction force $F_f$ to the rotation angle $\theta$.

$$\frac{\theta_f(s)}{F_f(s)} = -\frac{\frac{K_T\omega_n^2}{4c_1 A_p}\left(\frac{V_0}{\kappa RT_s}s + c_2\right)}{s(s^2 + 2\zeta\omega_n s + \omega_n^2)}. \tag{16}$$

Therefore, the total output of the valve-controlled actuator system is

$$\theta(s) = \theta_x(s) + \theta_f(s) = \frac{K_T\omega_n^2 x(s) - \frac{K_T\omega_n^2 F_f(s)}{4c_1 A_p}\left(\frac{V}{\kappa RT_s}s + c_2\right)}{s(s^2 + 2\zeta\omega_n s + \omega_n^2)}. \tag{17}$$

### 3.5. The Transfer Function of the Pneumatic Rotary Actuator Servo System

Because of the strong linearity of the selected proportional valve and the servo amplifier, the transfer function of them can be expressed as follows, respectively.

$$\frac{x_v(s)}{U(s)} = K_v \tag{18}$$

$$\frac{U(s)}{\theta_{in}(s) - \theta(s)} = K_a, \tag{19}$$

where $U$ is the drive voltage of the proportional valve, $K_v$ is the proportional valve gain, $\theta_{in}$ means the input angle, and $K_a$ expresses the servo amplifier gain.

According to Equations (17)–(19), the block diagram of the servo system can be obtained and is shown in Figure 6.

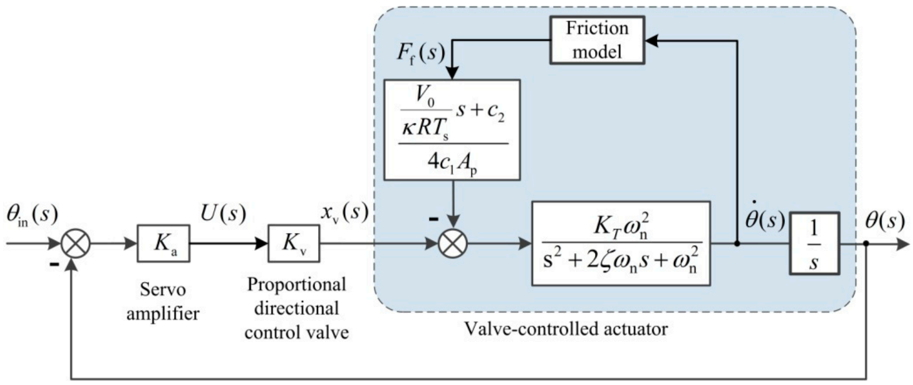


**Figure 6.** Block diagram of the pneumatic rotary actuator servo system.

Therefore, the open-loop transfer function of the pneumatic rotary actuator servo system is written as follows.

$$G(s) = \frac{K_a K_v K_T \omega_n^2}{s(s^2 + 2\zeta\omega_n s + \omega_n^2)}. \tag{20}$$

The constants in the model parameters are shown in Table 3.

**Table 3.** Constants in the model parameters.

| Parameter | Value |
|---|---|
| $A_p$ | $3.4636 \times 10^{-4}$ [m$^2$] |
| $C$ | 0.68 |
| $c_0$ | 0.21 |
| $d_f$ | 0.014 [m] |
| $J$ | $1.678 \times 10^{-3}$ [kg·m$^2$] |
| $\kappa$ | 1.4 |
| $m_p$ | 2.1 [kg] |
| $p_e$ | $1.013 \times 10^5$ [Pa] |
| $R$ | 287 [J/(kg·K)] |
| $T_s$ | 293 [K] |
| $V_0$ | $1.6767 \times 10^{-5}$ [m$^3$] |
| $W$ | $3.1415 \times 10^{-2}$ [m] |

## 4. Control Design

Figure 7 shows the control architecture of the pneumatic rotary actuator servo system, where the proportional valve and pneumatic rotary actuator are represented by the established model. In addition, the PD controller is used to adjust the deviation of the entire control system. However, if the system only uses the traditional PD control, the friction disturbance will seriously affect the output accuracy. Therefore, we use the friction feedforward compensation to compensate for the interference of friction. Besides, the evolutionary algorithm is used to optimize the PD controller parameters ($k_p$ and $k_d$), and can also be used to identify the friction parameters ($F_s$, $F_c$, $\dot{\theta}_s$ and $\sigma$) in Equation (10) to compensate for the friction disturbance. The identified friction model in Figure 7 is Equation (10) with new obtained parameters, which are identified by the evolutionary algorithm. $G_f(s)$ is the feedforward compensation term, which can be described by the form of transfer function.

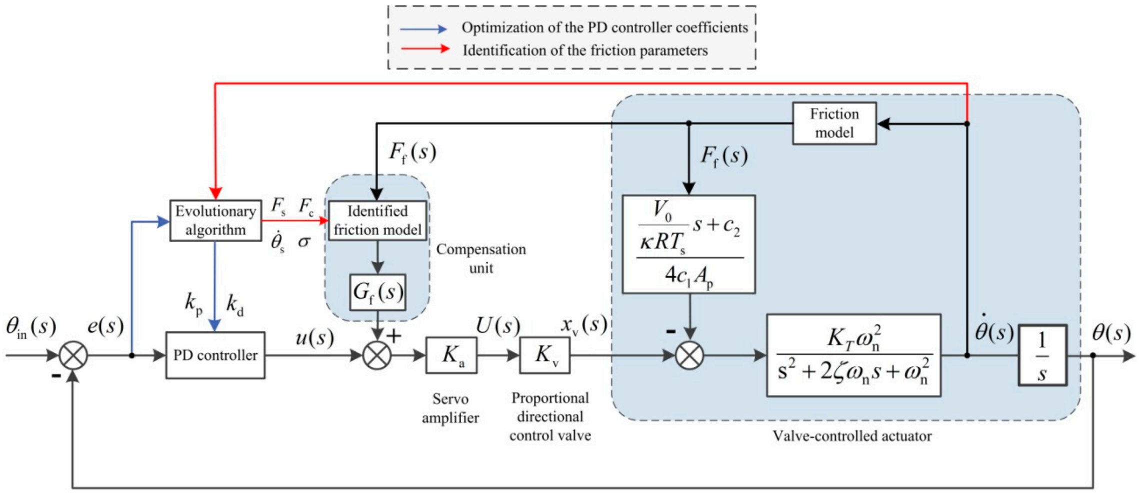


**Figure 7.** Control architecture.

## 4.1. PD Controller and Compensation Unit

PD control is a linear control method, which is based on the error $e(s)$ between the input angle $\theta_{in}(s)$ and the output angle $\theta(s)$, and there is

$$e(s) = \theta_{in}(s) - \theta(s). \tag{21}$$

The PD controller performs proportional and differential operations on the error $e(s)$, and adds the two operation results to obtain the control input $u(s)$. The expressions of the PD controller can be written as

$$u(s) = k_p e(s) + k_d s e(s), \tag{22}$$

where $k_p$ is the proportional coefficient, and $k_d$ is the differential coefficient. Through multiple feedback processes, the error will gradually shrink, which will improve the output accuracy.

Ideally, the friction value of the identified friction model is equal to that of the friction model. Therefore, the friction feedforward compensation satisfies the complete compensation condition:

$$G_f(s) K_a K_v - \frac{\frac{V_0}{\kappa R T_s} s + c_2}{4 c_1 A_p} = 0. \tag{23}$$

So the transfer function $G_f(s)$ of the feedforward compensation term is designed as

$$G_f(s) = \frac{\frac{V_0}{\kappa R T_s} s + c_2}{4 c_1 A_p K_a K_v}. \tag{24}$$

## 4.2. Evolutionary Algorithms

The parameters $k_p$, $k_d$, $F_s$, $F_c$, $\dot{\theta}_s$ and $\sigma$ are optimized offline by evolutionary algorithm (DE algorithm or GA). DE algorithm and GA are optimization algorithms based on swarm intelligence theory. They both can intelligently guide the optimization search through the group generated by cooperation and competition among individuals. The GA controls the parental hybridization according to the fitness value, and the probability of selecting the offspring after mutation is relatively large [24,35]. While the mutation vector in the DE algorithm is generated by the parent difference vector and intersects with the parent individual vector to generate a new individual vector, which will be directly compared with the parent individual [25,36]. It is obvious that the approximation effect of the DE algorithm is more significant than that of the GA.

Before describing these two algorithms, we use the following equation as the objective function of the parameter selection.

$$I = \sum_{n=1}^{Z} \left[ w_1 |e(n)| + w_2 \theta_{\text{in}}^2(n) \right] T_P, \tag{25}$$

where $I$ is the objective function; $n$ is the sampling times, and $n$ = 1, 2, 3, . . . , $Z$; $T_P$ represents the sampling period; $w_1$ and $w_2$ denote the weights.

4.2.1. Differential Evolution Algorithm

- Step 1: Generation of initial population

In the solution space, $M$ individuals are generated randomly and each individual $x_i^g$ is composed of a $N$-dimensional vector.

$$x_i^g = \left[ x_{i,1}^g, x_{i,2}^g, x_{i,3}^g, \ldots, x_{i,N}^g \right], \tag{26}$$

where $g$ stands for iteration counter, $g$ = 0, 1, 2, . . . , $G$; $i$ denotes individual number, and $i$ = 1, 2, 3, . . . , $M$. Each individual represents a set of parameters in the control architecture, where $n$ indicates the total number of the parameters. The $j$-th component vector of the $i$-th individual in the initial generation is as follows:

$$x_{i,j}^0 = b_{j-\min} + \text{rand}_{i,j}(0,1)\left(b_{j-\max} - b_{j-\min}\right), \tag{27}$$

where $j$ = 1, 2, 3, . . . , $N$, $b_{j-\min}$ and $b_{j-\min}$ represent upper and lower bounds of the $j$-th component vector, respectively, and $\text{rand}_{i,j}(0,1)$ means a random number between 0–1.

- Step 2: Mutation

In the $g$-th iteration, three individuals $x_{p1}^g$, $x_{p2}^g$ and $x_{p3}^g$ were randomly selected from the population, and $i \neq p1 \neq p2 \neq p3$. Then the mutation vectors are generated by the following process.

$$h_{i,j}^{g+1} = x_{p1,j}^g + F\left(x_{p2,j}^g - x_{p3,j}^g\right), \tag{28}$$

where $x_{p2,j}^g - x_{p3,j}^g$ is a differential component vector, and this difference operation is the key to the DE algorithm. $p1$, $p2$ and $p3$ are random integers, $F$ is known as a scaling factor.

- Step 3: Crossover

Crossover is to increase population diversity, which can be expressed as follows

$$v_{i,j}^{g+1} = \begin{cases} h_{i,j}^{g+1}, & \text{rand } l_{i,j} \leq CR \\ x_{i,j}^g, & \text{rand } l_{i,j} > CR \end{cases}, \tag{29}$$

where rand $l_{i,j}$ is a random number between 0–1, $CR$ is a crossover rate, and $CR \in [0,1]$.

- Step 4: Selection

In order to determine whether $x_i^g$ is the next generation member, the fitness function values of trial vector $v_i^{g+1}$ and target vector $x_i^g$ are compared.

$$x_i^{g+1} = \begin{cases} v_i^{g+1}, & f(v_i^{g+1}) < f(x_i^g) \\ x_i^g, & f(v_i^{g+1}) \geq f(x_i^g) \end{cases}, \tag{30}$$

where $f(x)$ is the fitness function. Therefore, under the condition that the number of individuals is constant, the population can obtain better performance or maintain the previous fitness value.

- Step 5: Iteration and end condition

Run the operation of steps 2–4 repeatedly until the maximum number of iterations is reached ($g = G$). Then we can get the best result.

4.2.2. Genetic Algorithm

- Step 1: Coding scheme

$N$ binary strings with 10 bits in length are used to represent the identified parameters respectively. Then the $N$ strings are connected into a complete chromosome to form the individual in the population.

- Step 2: Initial population formation

A set of parameters that need to be identified are selected as the initial parameters. Then we extend this set of parameters around the left and right sides to form an extended population search space. The initial population is assigned by a computer. First, generate random numbers that are evenly distributed between [0,1]. Then specify that the generated random numbers between [0,0.5] represents 0, and the numbers between [0.5,1] represents 0.

- Step 3: Fitness function design

Each individual in the population is decoded into the corresponding parameter value, and the cost function value $J$ and the fitness function value $f$ are obtained by using this parameter. There is $f = \frac{1}{J}$.

- Step 4: Evolutionary process

Selection: Produce a new generation population by selecting operation.
Crossover: Implement crossover operation with the cross probability $P_c$.
Mutation: Implement mutation operation with the mutation probability $P_m$.

According to fitness function values, we adopt optimal preservation and regenerate individual strategy. That is to say, when the ratio of the average fitness of individuals to the maximum fitness of the current population reaches a certain range, the best individuals are retained and the rest of the individuals are regenerated. The former makes the whole evolution process move towards the optimization direction, and the latter overcomes the precocity phenomenon in genetic search to some extent.

- Step 5: Iteration and end condition

Repeat steps 3 and 4 until the maximum number of iteration is reached. Then the optimal results are obtained after decoding.

## 5. Experimental Results and Analysis

Figure 8 shows the experimental platform of the pneumatic rotary actuator servo system. We can compare and verify the control accuracy of different control strategies by changing the input signal and the load moment. The system control architecture adopts four control strategies respectively: the traditional PD control without friction compensation, the PD control with friction feedforward compensation without evolutionary algorithm tuning, the PD control with friction feedforward compensation based on the DE algorithm and the PD control with friction feedforward compensation based on the GA. In the traditional PD control strategy, we take $k_p$ and $k_d$ obtained from the trial and error method as the two parameters of the controller. For the second strategy, we use the same $k_p$ and $k_d$, the friction parameters ($F_s$, $F_c$, $\dot{\theta}_s$ and $\sigma$) in the compensation unit adopts the parameter values obtained in Section 3.3, and all parameters in this strategy are not adjusted by evolutionary algorithm and directly used in the system test. In the other two control methods, first we use the control algorithm (DE algorithm or GA) to optimize $k_p$ and $k_d$, and identify the friction parameters ($F_s$, $F_c$, $\dot{\theta}_s$ and $\sigma$) by MATLAB, and then we use the obtained parameters in the servo system. Through experimental contrast of the four control strategies, we can clearly contrast the effect of the friction feedforward compensation and two different control algorithms (DE algorithm and GA).

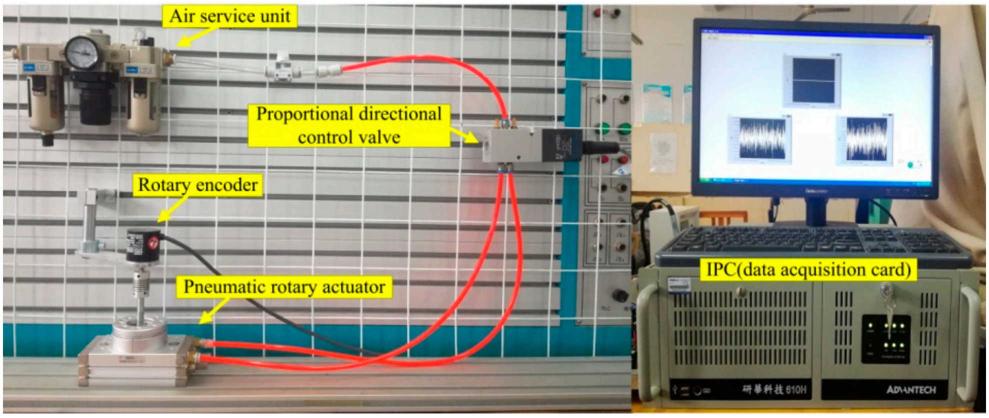


**Figure 8.** Experimental platform of the pneumatic rotary actuator servo system.

### 5.1. Position Tracking Experiment

In the position tracking experiment, we set the supply pressure $p_s$ as 0.6 MPa. In both algorithms, the number of individuals was 30, the range of the parameter $k_p$ was [–5,20], the range of the parameter $k_d$ was $[-1,1]$, and the weights were taken as $w_1 = 0.999$ and $w_2 = 0.001$. Specifically, in the GA, $P_c = 0.9$, and $P_m = 0.033$.

After 50 iterations, we got the PD controller parameters optimized by evolutionary algorithm. Figure 9 shows the optimization process of $k_p$ and $k_d$ by the DE algorithm and the GA. Then each set of the controller parameters was used in the friction parameter identification of the corresponding algorithm, and the friction parameters tested in Section 3.3 were selected as the initial parameters. The identification processes of different algorithms are shown in Figure 10. Finally, the controller parameters and the friction parameters were applied to the pneumatic rotary actuator servo system shown in Figure 8. By giving the system a sinusoidal signal with a magnitude of 20 and a frequency of 0.5 Hz, we obtained the position tracking performance of the pneumatic rotary actuator. Figure 11 shows the position tracking results of the pneumatic rotary actuator under three control strategies, where Figure 11a shows the angle contrast curve, Figure 11b describes the error contrast curve, and Figure 11c shows the angular velocity contrast curve.

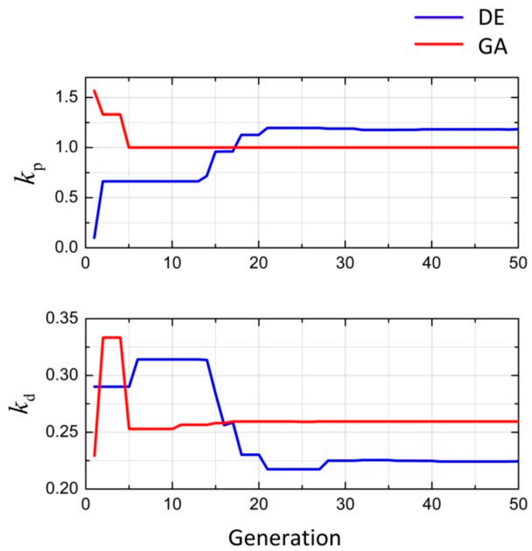


**Figure 9.** Optimization process of $k_p$ and $k_d$ in the position tracking experiment.

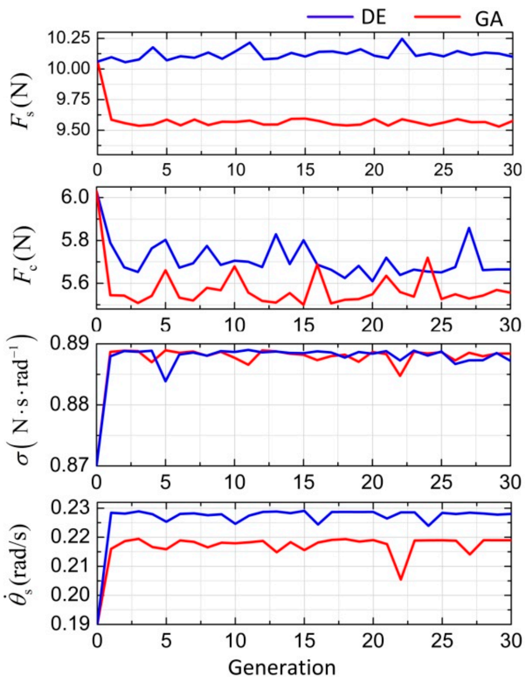


**Figure 10.** Identification process of the friction parameters in the position tracking experiment.

In order to facilitate contrast and analysis, the unit of the angle $\theta$ in experiment is expressed by degrees. In the figures, PD with friction compensation stands for the PD control with friction feedforward compensation without evolutionary algorithm tuning, DE-PD denotes the PD control with friction feedforward compensation based on the DE algorithm, and GA-PD represents the PD control with friction feedforward compensation based on the GA.

As shown in Figure 11b, the maximum angular errors of four control strategies (traditional PD control, PD with friction compensation, DE-PD and GA-PD control) were 0.85°, 0.35°, 0.1° and 0.25° respectively. The error curve of the PD control with friction feedforward compensation without evolutionary algorithm tuning continued the error fluctuation frequency of the traditional PD control strategy because they used the same controller parameters. This method can reduce the error to a certain extent, but, since the controller parameters and friction parameters were not optimized, the error values were still relatively large. While the friction feedforward compensation based on evolutionary algorithm greatly reduced the position tracking error of the pneumatic rotary actuator, and the DE-based case had the best performance. Figure 11c shows the velocity fluctuations of the pneumatic rotary actuator with different control algorithms, revealing that the actuator with the DE-PD control strategy was more stable.

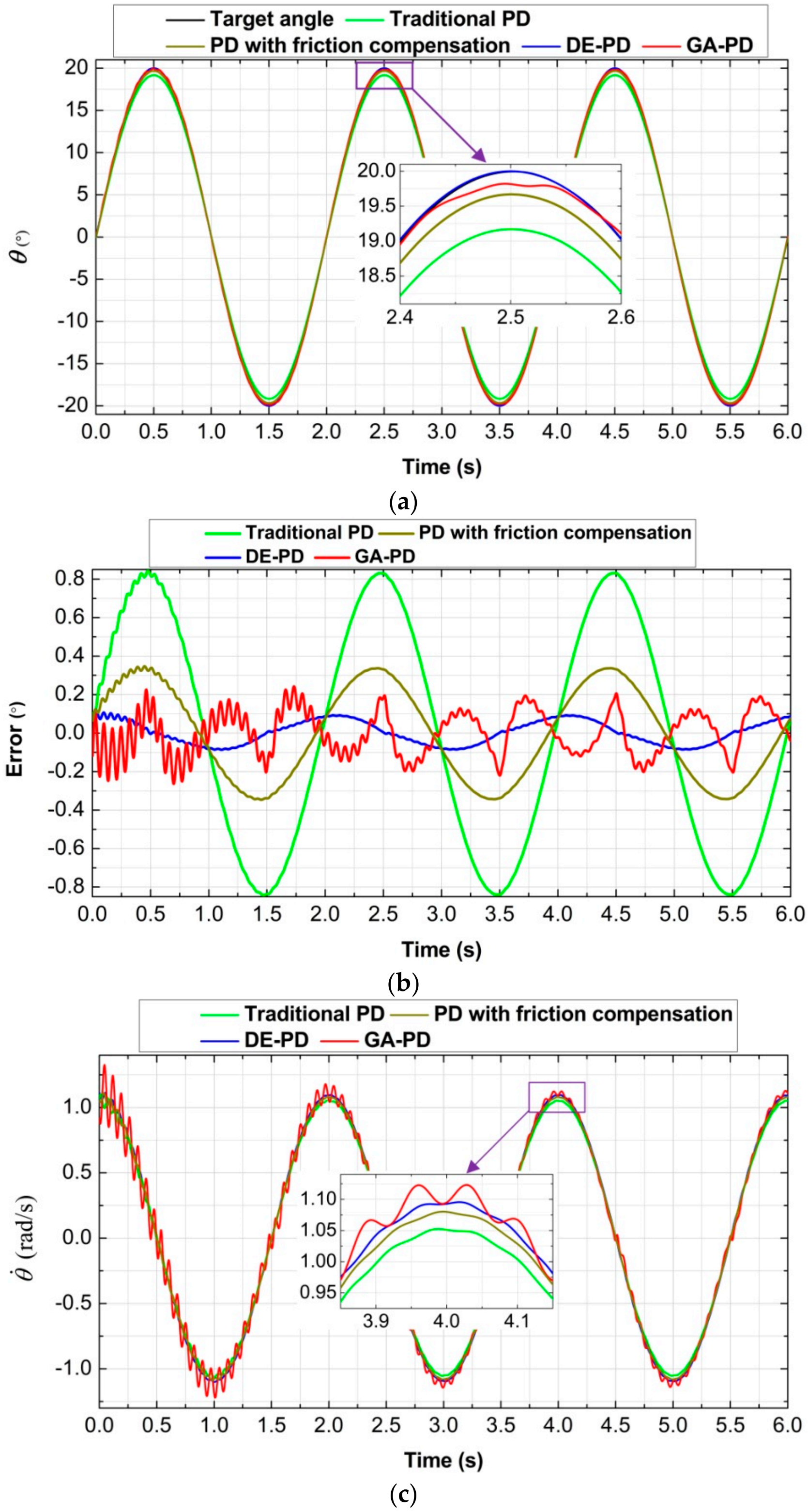


**Figure 11.** Position tracking performances under four control strategies. (**a**) Angle contrast curve; (**b**) error contrast curve; and (**c**) angular velocity contrast curve.

### 5.2. Positioning Experiment

By setting a constant angle signal, we carried out the positioning experiment and obtained the positioning performance of the pneumatic rotary actuator. Figures 12 and 13 show the optimization process of the PD controller coefficients and the identification process of the friction parameters respectively. The positioning performances of the pneumatic rotary actuator under three control strategies are shown in Figure 14, including the angle contrast curve, the error contrast curve and the angular velocity contrast curve.

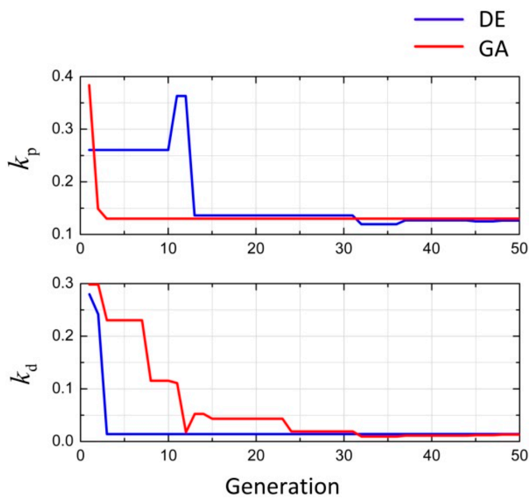


**Figure 12.** Optimization process of $k_p$ and $k_d$ in the positioning experiment.

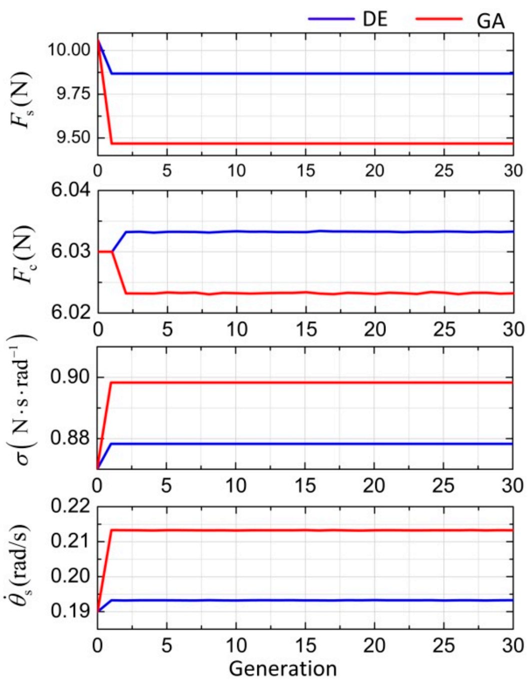


**Figure 13.** Identification process of the friction parameters in the positioning experiment.

As shown in Figure 14b, the maximum angular errors of four control strategies (traditional PD control, PD with friction compensation, DE-PD and GA-PD control) were 0.225°, 0.107°, 0.003° and 0.075° respectively. This result shows that the friction feedforward compensation based on evolutionary algorithm improved the positioning accuracy of the system, and that the DE-based case achieved higher accuracy. Figure 14c shows the velocity fluctuations of the pneumatic rotary actuator when input angle was a constant, and reveals that the pneumatic rotary actuator run smoothly when the system tended to a steady state. Also, as shown in Figures 9, 10, 12 and 13, the iterative processes of the algorithms tend to be stable, which ensures that the evolutionary algorithm-based case does not go unstable.

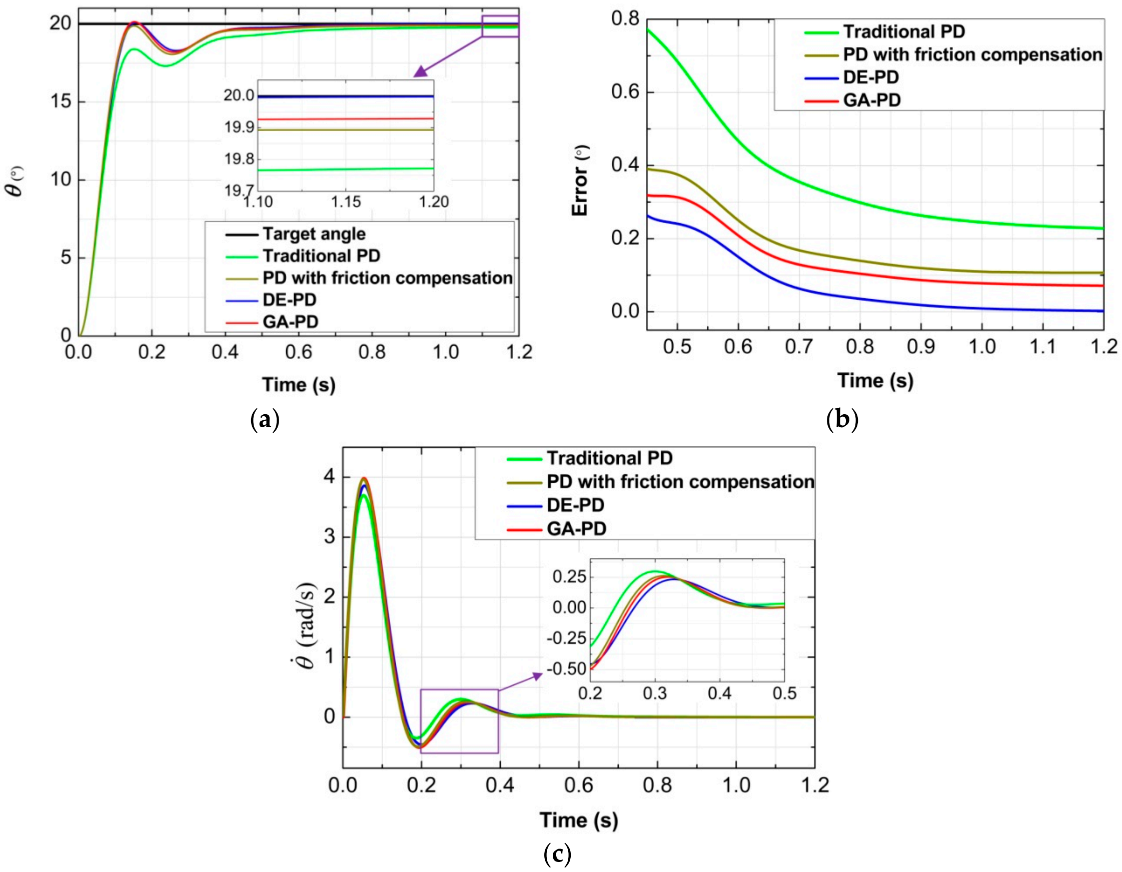


**Figure 14.** Position tracking performances under four control strategies. (**a**) Angle contrast curve; (**b**) error contrast curve; and (**c**) angular velocity contrast curve.

### 5.3. Stability Experiment with Load

The stability of the control system was tested by fixing a 2-kg mass block on the rotary table of the pneumatic rotary actuator. Then the moment of inertia $J$ changed to $3.356 \times 10^{-3}$ kg·m$^2$. The mass block increased the moment of inertia of the rotary table, which affected the position accuracy of the system. Using the same method, first we used different control strategies to tune the controller coefficients and friction parameters of the system respectively, and then substituted them into the system for testing. Figure 15 describes the position tracking performance of the pneumatic rotary actuator with a load. Figure 16 shows the positioning performance of the actuator with a load.

As shown in Figure 15b, the maximum angular errors of four control strategies (traditional PD control, PD with friction compensation, DE-PD and GA-PD control) were 0.885°, 0.357°, 0.125°, and 0.27° respectively. In Figure 16b, the steady-state errors of the pneumatic rotary actuator were 0.25°, 0.125°, 0.025° and 0.1° respectively. Compared with Figures 11b and 14b, the errors of the actuator with a load are relatively large. This is because the increase of the load leads to an increase in the dead zone characteristic, which means that the micro pressure difference in the actuator chambers is difficult to change the rotation angle when the target angle is approached. Even so, the friction feedforward compensation based on evolutionary algorithm can still keep the error within a small range, which well verifies the strong stability of the control system.

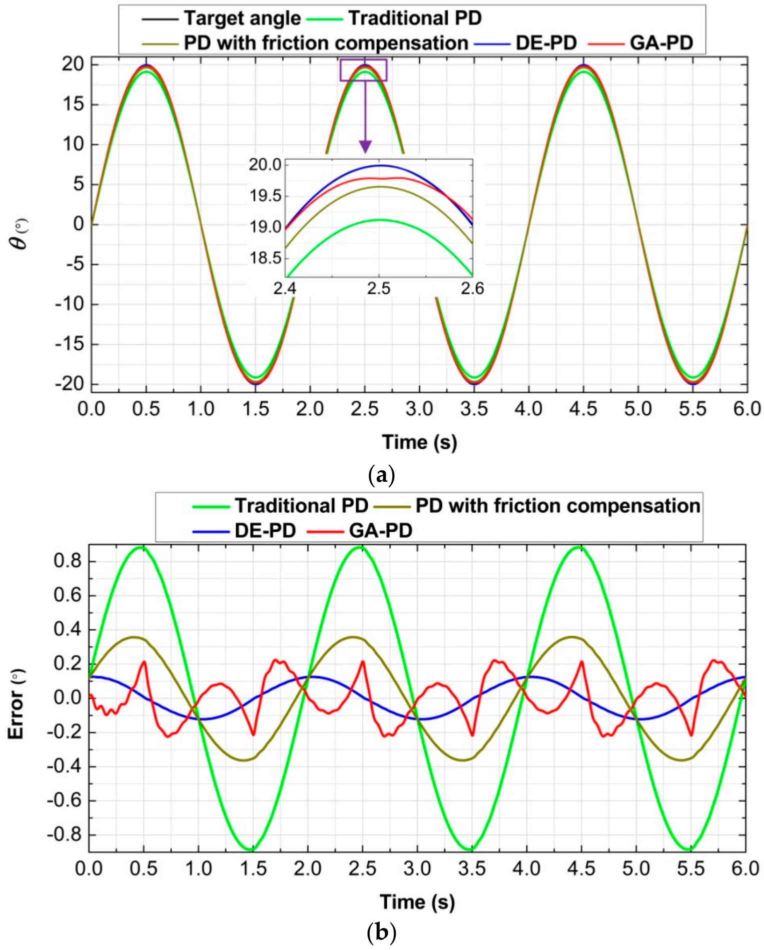


**Figure 15.** Position tracking performance in the stability experiment. (**a**) Angle contrast curve; (**b**) error contrast curve.

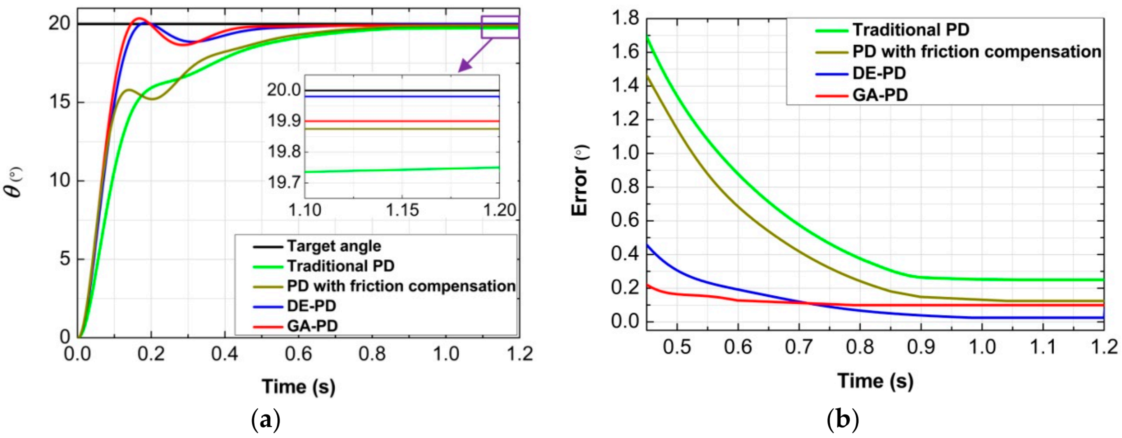


**Figure 16.** Positioning performance in the stability experiment. (**a**) Angle contrast curve; (**b**) error contrast curve.

The allowable load of the pneumatic rotary actuator is 48 N [37]. We tested the angle errors of the system when the load is 1 kg, 2 kg, 3 kg and 4 kg. Figure 17 shows their angle errors under different loads, and clearly describes the trends of errors. The result reveals that the evolutionary algorithm-turned errors are relatively small and have good stability, and that the DE-based case has higher accuracy. In conclusions, it is the smoothness and accuracy of the algorithm iterative process that make the system under different loads still have stable performances.

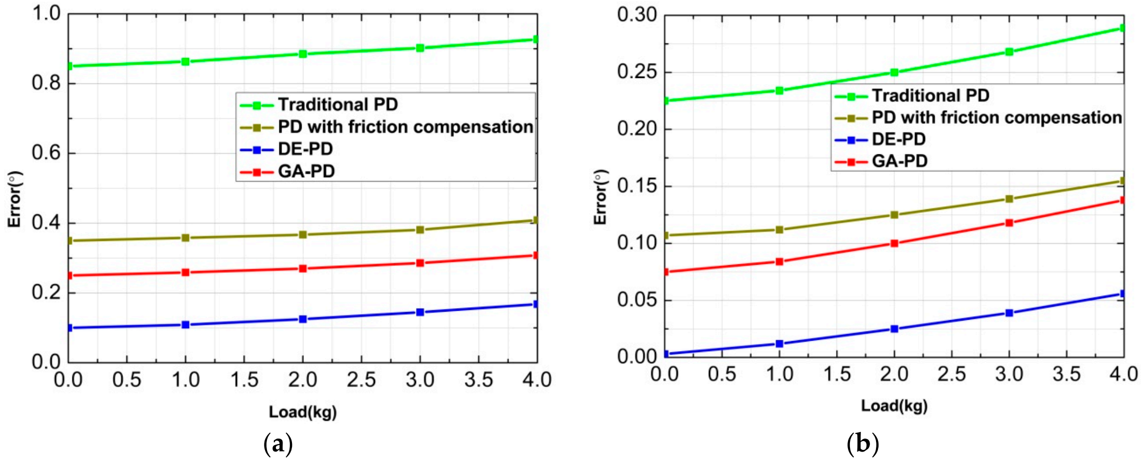


**Figure 17.** Angle errors under different loads. (**a**) Position tracking error; (**b**) positioning error.

## 6. Conclusions

In order to improve the position accuracy of the pneumatic rotary actuator servo system, the modeling of the system and the design of the evolutionary algorithm-based friction feedforward compensation control architecture were carried out and verified by the experiments. Firstly, basic equations of the valve-controlled actuator were derived and linearized in the middle position, and the transfer function of the system was further obtained. Then, the evolutionary algorithm-based friction feedforward compensation control architecture was designed, which includes the optimization of the controller coefficients and the identification of the friction parameters. Finally, in the position tracking experiment, the positioning experiment and the stability experiment with load, the control performances of four control strategies (the traditional PD control, the PD control with friction feedforward compensation without evolutionary algorithm tuning, the PD control with friction feedforward compensation based on the DE algorithm and the PD control with friction feedforward compensation based on the GA) were contrasted and analyzed, and the following conclusions were obtained:

(1) The PD control with friction feedforward compensation without evolutionary algorithm tuning can reduce the system error to a certain extent. However, since the controller parameters and friction parameters were not optimized, the error values were still relatively large.

(2) The friction feedforward compensation based on evolutionary algorithm greatly improved the position tracking performance for the sinusoidal signal, and the DE-based case had better control accuracy and smaller velocity fluctuations.

(3) The friction feedforward compensation based on evolutionary algorithm greatly improved the positioning performance when the input angle was a constant, and the DE-based case achieved higher accuracy.

(4) Although the existence of the load affected the tracking and positioning effects, the system with the evolutionary algorithm-based friction feedforward compensation still maintained high accuracy and strong stability.

**Author Contributions:** Conceptualization, K.L. and Y.Z.; Data curation, S.W. and H.Y.; Funding acquisition, Y.Z.; Investigation, K.L.; Project administration, Y.Z.; Supervision, S.W.; Writing—original draft, K.L.; Writing—review & editing, K.L., Y.Z. and H.Y.

**Funding:** The research reported in the article was funded by the Fundamental Research Funds for Henan Province Colleges and Universities (Grant No. NSFRF140120); Henan Province Science and Technology Key Project (Grant No. 172102310674); the Doctor Foundation of Henan Polytechnic University (Grant No. B2012-101); the Science and Technology Research Projects of Education Department of Henan province (Grant No. 14B460033); The Construction Project of the Case Library Course for Graduate Students of Henan Polytechnic University (Grant No. 2016YAL09).

**Acknowledgments:** The authors would like to thank Henan Polytechnic University for its support. The authors are sincerely grateful to the reviewers for their valuable review comments, which substantially improved the paper.

**Conflicts of Interest:** The authors declare no conflicts of interest.

## References

1. Ning, F.; Shi, Y.; Cai, M.; Wang, Y.; Xu, W. Research Progress of Related Technologies of Electric-Pneumatic Pressure Proportional Valves. *Appl. Sci.* **2017**, *7*, 1074. [CrossRef]
2. Shi, Y.; Wang, Y.; Cai, M.; Zhang, B.; Zhu, J. An aviation oxygen supply system based on a mechanical ventilation model. *Chin. J. Aeronaut.* **2018**, *31*, 197–204. [CrossRef]
3. Niu, J.; Shi, Y.; Cao, Z.; Cai, M.; Chen, W.; Zhu, J.; Xu, W. Study on air flow dynamic characteristic of mechanical ventilation of a lung simulator. *Sci. Chin. Technol. Sci.* **2017**, *60*, 243–250. [CrossRef]
4. Zhang, Y.M.; Cai, M.L. Overall life cycle comprehensive assessment of pneumatic and electric actuator. *Chin. J. Mech. Eng.* **2014**, *27*, 584–594. [CrossRef]
5. Nie, S.; Liu, X.; Yin, F.; Ji, H.; Zhang, J. Development of a High-Pressure Pneumatic On/Off Valve with High Transient Performances Direct-Driven by Voice Coil Motor. *Appl. Sci.* **2018**, *8*, 611. [CrossRef]
6. Niu, J.; Shi, Y.; Cai, M.; Cao, Z.; Wang, D.; Zhang, Z.; Zhang, X.D. Detection of Sputum by Interpreting the Time-frequency Distribution of Respiratory Sound Signal Using Image Processing Techniques. *Bioinformatics* **2017**, *34*, 820–827. [CrossRef] [PubMed]
7. Shi, Y.; Zhang, B.; Cai, M.; Xu, W. Coupling Effect of Double Lungs on a VCV Ventilator with Automatic Secretion Clearance Function. *IEEE/ACM Trans. Comput. Biol. Bioinform.* **2017**. [CrossRef] [PubMed]
8. Shi, Y.; Hao, L.; Cai, M.; Wang, Y.; Yao, J.; Li, R.; Feng, Q.; Li, Y. High-precision diameter detector and three-dimensional reconstruction method for oil and gas pipelines. *J. Petrol. Sci. Eng.* **2018**, *165*, 842–849. [CrossRef]
9. Saravanakumar, D.; Mohan, B.; Muthuramalingam, T. A review on recent research trends in servo pneumatic positioning systems. *Precis. Eng.* **2017**, *49*, 481–492. [CrossRef]
10. Kim, D.-S.; Lee, W.-H. Development of the Pneumatic Rotary Actuator for Marine Winch. *J. Korean Soc. Mar. Eng.* **2004**, *28*, 354–360.
11. Chen, S.Y.; Gong, S.S. Speed tracking control of pneumatic motor servo systems using observation-based adaptive dynamic sliding-mode control. *Mech. Syst. Signal Process.* **2017**, *94*, 111–128. [CrossRef]
12. Ren, S.; Cai, M.; Shi, Y.; Xu, W.; Zhang, X.D. Influence of bronchial diameter change on the airflow dynamics based on a pressure-controlled ventilation system. *Int. J. Numer. Methods Biomed. Eng.* **2017**, *34*, e2929. [CrossRef] [PubMed]
13. Valdiero, A.C.; Ritter, C.S.; Rios, C.F.; Rafikov, M. Nonlinear mathematical modeling in pneumatic servo position applications. *Math. Probl. Eng.* **2011**, *2011*, 472903. [CrossRef]
14. Armstrong-Hélouvry, B.; Dupont, P.; Wit, C.C.D. A survey of models, analysis tools and compensation methods for the control of machines with friction. *Automatica* **1994**, *30*, 1083–1138. [CrossRef]
15. Rad, C.-R.; Hancu, O. An improved nonlinear modelling and identification methodology of a servo-pneumatic actuating system with complex internal design for high-accuracy motion control applications. *Simul. Model. Pract. Theory* **2017**, *75*, 29–47. [CrossRef]
16. Gao, X.; Feng, Z.J. Design study of an adaptive Fuzzy-PD controller for pneumatic servo system. *Control Eng. Pract.* **2005**, *13*, 55–65. [CrossRef]
17. Meng, D.; Tao, G.; Liu, H.; Zhu, X. Adaptive robust motion trajectory tracking control of pneumatic cylinders with lugre model-based friction compensation. *Chin. J. Mech. Eng.* **2014**, *27*, 802–815. [CrossRef]
18. Sobczyk, M.R.; Gervini, V.I.; Perondi, E.A.; Cunha, M.A.B. A Continuous Version of the LuGre Friction Model Applied to the Adaptive Control of a Pneumatic Servo System. *J. Frankl. Inst.* **2016**, *353*, 3021–3039. [CrossRef]
19. Guenther, R.; Perondi, E.A.; Depieri, E.R.; Valdiero, A.C. Cascade controlled pneumatic positioning system with LuGre model based friction compensation. *J. Braz. Soc. Mech. Sci. Eng.* **2006**, *28*, 48–57. [CrossRef]
20. Xu, J.; Qiao, M.; Wang, W.; Miao, Y. *Fuzzy PID Control for Ac Servo System Based on Stribeck Friction Model*; Strategic Technology (IFOST): Ulsan, South Korea, 2011; pp. 706–711.
21. Márton, L.; Fodor, S.; Sepehri, N. A practical method for friction identification in hydraulic actuators. *Mechatronics* **2011**, *21*, 350–356. [CrossRef]

22. Castro, R.D.; Todeschini, F.; Rui, E.A.; Savaresi, S.M.; Corno, M.; Freitas, D. Adaptive-robust friction compensation in a hybrid brake-by-wire actuator. *Proc. Inst. Mech. Eng. Part I J. Syst. Eng.* **2014**, *228*, 769–786. [CrossRef]
23. Zhang, Y.; Li, K.; Wei, S.; Wang, G. Pneumatic Rotary Actuator Position Servo System Based on ADE-PD Control. *Appl. Sci.* **2018**, *8*, 406. [CrossRef]
24. Dangor, M.; Dahunsi, O.A.; Pedro, J.O.; Ali, M.M. Evolutionary algorithm-based PID controller tuning for nonlinear quarter-car electrohydraulic vehicle suspensions. *Nonlinear Dynam.* **2012**, *78*, 2795–2810. [CrossRef]
25. Pedro, J.O.; Dangor, M.; Dahunsi, O.A.; Ali, M.M. Differential Evolution-Based PID Control of Nonlinear Full-Car Electrohydraulic Suspensions. *Math. Probl. Eng.* **2013**, *2013*, 532–548. [CrossRef]
26. Jiao, Z.; Qu, B.; Xu, B. Application of Genetic Algorithm to Friction Compensation in Direct Current Servo Systems. *J. Xian Jiaotong Univ.* **2007**, *8*, 017.
27. Jiao, Z.; Qu, B.; Xu, B. DC servo motor friction compensation using a genetic algorithm. *J. Tsinghua Univ.* **2007**, S2.
28. Shi, Y.; Cai, M. Working characteristics of two kinds of air-driven boosters. *Energy Convers. Manag.* **2011**, *52*, 3399–3407. [CrossRef]
29. Shi, Y.; Wu, T.; Cai, M.; Wang, Y.; Xu, W. Energy conversion characteristics of a hydropneumatic transformer in a sustainable-energy vehicle. *Appl. Energy* **2016**, *171*, 77–85. [CrossRef]
30. Shi, Y.; Wang, Y.; Liang, H.; Cai, M. Power characteristics of a new kind of air-powered vehicle. *Int. J. Energy Res.* **2016**, *40*, 1112–1121. [CrossRef]
31. Shi, Y.; Zhang, B.; Cai, M.; Zhang, X.D. Numerical simulation of volume-controlled mechanical ventilated respiratory system with 2 different lungs. *Int. J. Numer. Methods Biomed. Eng.* **2017**, *33*, e2852. [CrossRef] [PubMed]
32. Ren, S.; Shi, Y.; Cai, M.; Xu, W. Influence of secretion on airflow dynamics of mechanical ventilated respiratory system. *IEEE/ACM Trans. Comput. Biol. Bioinform.* **2018**, *PP*, 1. [CrossRef] [PubMed]
33. Peter, B. *Pneumatic Drives System Design, Modeling and Control*; Springer: Berlin/Heidelberg, Germany, 2007.
34. Sanville, F. A new method of specifying the flow capacity of pneumatic fluid power valves. *Hydraul. Pneum. Power* **1971**, *17*, 120–126.
35. Qiu, Z.C.; Shi, M.L.; Wang, B.; Xie, Z.W. Genetic algorithm based active vibration control for a moving flexible smart beam driven by a pneumatic rod cylinder. *J. Sound Vib.* **2012**, *331*, 2233–2256. [CrossRef]
36. Andromeda, T.; Yahya, A.; Samion, S.; Baharom, A.; Hashim, N.L. Differential evolution for optimization of PID gain in Electrical Discharge Machining control system. *Trans. Can. Soc. Mech. Eng.* **2013**, *37*, 293–301. [CrossRef]
37. Operation Manual of Pneumatic Rotary Actuator MSQ. Available online: http://www.smcworld.com/assets/manual/en-jp/files/MSQ-E.pdf (accessed on 2 September 2018).